Editors' Suggestion   Featured in Physics

Emergent Collective Motion of Self-Propelled Condensate Droplets

Marcus Lin,[1] Philseok Kim,[2] Sankara Arunachalam,[1] Rifan Hardian,[1] Solomon Adera,[2]
Joanna Aizenberg,[2,3,*] Xi Yao [2,4,†] and Dan Daniel [1,‡]

[1]*Division of Physical Sciences and Engineering, King Abdullah University of Science and Technology (KAUST),
Thuwal 23955-6900, Saudi Arabia*
[2]*John A. Paulson School of Engineering and Applied Sciences, Harvard University, Cambridge, Massachusetts 02138, USA*
[3]*Department of Chemistry and Chemical Biology, Harvard University, Cambridge, Massachusetts 02138, USA*
[4]*Department of Biomedical Sciences, City University of Hong Kong, Hong Kong, China*

Recently, there is much interest in droplet condensation on soft or liquid or liquidlike substrates. Droplets can deform soft and liquid interfaces resulting in a wealth of phenomena not observed on hard, solid surfaces (e.g., increased nucleation, interdroplet attraction). Here, we describe a unique collective motion of condensate water droplets that emerges spontaneously when a solid substrate is covered with a thin oil film. Droplets move first in a serpentine, self-avoiding fashion before transitioning to circular motions. We show that this self-propulsion (with speeds in the 0.1–$1\ \text{mm s}^{-1}$ range) is fueled by the interfacial energy release upon merging with newly condensed but much smaller droplets. The resultant collective motion spans multiple length scales from submillimeter to several centimeters, with potentially important heat-transfer and water-harvesting applications.

With its long and illustrious history, the study of condensate droplets (sometimes called breath figures) has captured the imaginations of many scientists, including Lord Rayleigh and C.V. Raman [1–5]. Optimizing the condensation process has important heat-transfer and water-harvesting applications [6,7], and the ability to control the size of condensate droplets is useful when templating micro- or nanostructured materials [8] and producing structural colors [2,9].

Recently, there is much interest in understanding droplet condensation on lubricated surfaces [10–14] for enhanced heat-transfer and water-collection applications [10,15–17]. Water droplets are highly mobile on lubricated surfaces [18–20] because the lubricant film (typically silicone or fluorinated oils) prevents direct contact of the droplet with the underlying solid substrate [21,22]. The lubricant also tends to wrap around droplets forming menisci or wetting ridges around them, which can overlap and give rise to interdroplet capillary attraction (akin to the Cheerios effect [23]) and faster droplet coalescence [13,24,25]. This process frees up new areas for droplet renucleation and therefore increases heat-transfer rate. Previous reports of interdroplet attraction is confined to neighboring droplets

with droplet displacement limited to a millimeter or less with no long-range collective motion [10,13,24,26].

Here, we report the spontaneous emergence of complex collective motion of condensate droplets whose displacements span several centimeters or more, i.e., many times the droplet diameters. Droplets ranging from tens of microns to several millimeters in size move laterally in a serpentine, self-avoiding fashion. At a later stage when the *local* lubricant film is depleted, the serpentine motion transitions to circular motions. As the lubricant film is being redistributed by the moving droplets, the droplets continually switch between serpentine and circular motions in a collective fashion—a classic example of emergence where complexity arises from interactions of its parts [27,28]. The phenomenon described here is an interesting example of active matter [29–31] whereby autonomous droplet motions are fueled by the energy release from condensation [32], as opposed to the typical chemical reactions or Marangoni effects [31,33–37].

We start by cooling a micropillar surface (hexagonal array with diameter $d = 2\ \mu\text{m}$, pitch $p = 10\ \mu\text{m}$, and height $h_p = 9\ \mu\text{m}$) lubricated with a thin film of fluorinated oil (overlayer thickness $h_o = 5\ \mu\text{m}$, viscosity $\eta = 53\ \text{mPa.s}$) to a temperature of $T = 4\ °\text{C}$. Throughout the experiments described here, the ambient temperature was kept at $22\ °\text{C}$ and the room humidity between 40% and 60%. Within the first minute, water started to condense on the surface, and we observed capillary attraction between neighboring droplets (submillimetric and *similarly* sized) [Figs. 1(a) and 1(b)]. This occurs when their wetting ridges overlap resulting in a nonaxisymmetric meniscus around each droplet and hence a
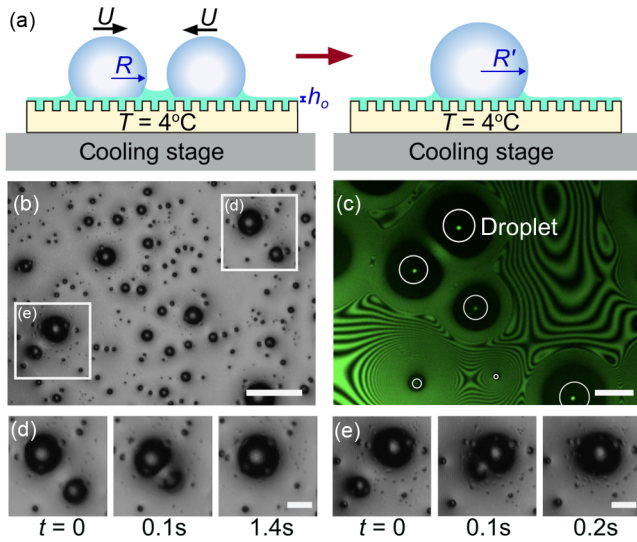
FIG. 1. (a) Initial interdroplet attraction and coalescence on a cooled lubricated surface. (b) Coalescence and subsequent recondensation results in polydisperse droplet sizes. Scale bar is 2 mm. (c) Nonaxisymmetric menisci (dark regions around each droplet) as observed using reflection interference contrast microscopy. Scale bar is 0.1 mm. (d),(e) Time series for the two boxed regions in (b). Scale bars are 0.15 mm.

net attractive force akin to the Cheerios effect [13,23,24]. The deformation to the lubricant interface can be visualized by shining monochromatic light with wavelength $\lambda = 561$ nm from below, a technique known as reflection interference contrast microscopy [Fig. 1(c)] [21,38]; the bright and dark fringes correspond to different lubricant heights, with a step height $|\Delta h| = \lambda/4n_o \approx 100$ nm between neighboring bright and dark fringes ($n_o = 1.3$ is the refractive index of the lubricant). The size of wetting ridge (dark region around the droplet outline) is comparable to that of the droplet [see Supplemental Material (SM), Fig. S1 [39]]. Hence, droplets that are several diameters apart can move toward each other before coalescing [Figs. 1(d) and 1(e); SM Video S1 [39]]. The details of this interdroplet attraction have been described by many others [13,24,41]. Here, we would like to emphasize that this process naturally leads to polydisperse droplet sizes [Fig. 1(b)], which is key to understanding the mechanism behind the collective droplet motion described below.

After 27 m of cooling, one droplet becomes much larger than its neighbors and starts moving in a serpentine, self-avoiding fashion, as imaged using an infrared (IR) camera [Figs. 2(a) and 2(b); SM Videos S2,S3 [39]]. Unlike the droplet propulsion described previously, which is limited to submillimetric distances, the serpentine motion here can cover much larger distances. For example, droplet A in Fig. 2(b)–1 traversed a distance of 6 cm within 12 m with an average lateral velocity of $U_L = 0.1$ mm s^{-1} [Fig. 2(c)]; as the droplet swept through its much smaller neighbors, its radius R more than triples from less than 0.4 mm to 1.3 mm
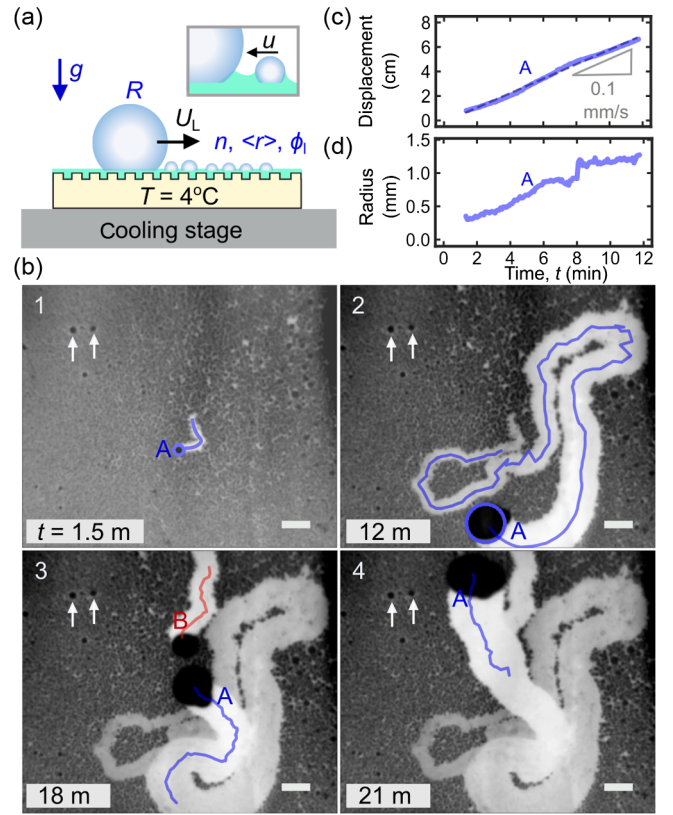

FIG. 2. (a) Schematic and (b) IR imaging (2 mm scale bars) showing the self-propelled serpentine motion of condensate droplets on a cooled lubricated micropillar surface. Droplet size and position are tracked automatically using Hough transform [42]. Increase in (c) displacement and (d) radius with time for droplet A for the first 12 m of motion. $t = 0$ m corresponds to the start of droplet A motion which occurs after 27 m of cooling.

[Fig. 2(d)]. In contrast, the stationary droplets indicated by arrows in Fig. 2(b) hardly grow in size.

The self-propelled droplets also preferentially avoid their own and each other's paths, i.e., self-avoiding [see how droplet B avoids the path of droplet A in Fig. 2(b)–3]. The droplets can only intersect their own paths once there is sufficient recondensation (which consequently turn from white to gray). The self-propelled droplets can collide into each other and coalesce into a larger droplet that starts its own serpentine motion [Fig. 2(b)–4]. Since we positioned our surface horizontally (unlike in previous studies [10,43]), gravity plays little role as long as $R \ll l_c$, where $l_c = \sqrt{\gamma/\rho g} = 2.7$ mm is the capillary length.

The origin of this serpentine motion is once again capillary attraction—between one large droplet and multiple smaller droplets—mediated by overlapping wetting ridges [Fig. 2(a) inset; SM Fig. S2 [39]]. The capillary force arising from the nonaxisymmetric menisci is notoriously difficult to model mathematically with analytic solutions only when droplets are far apart [23,44,45]. Here, we derive a simple expression for U_L by using energy balance arguments. As the large droplet of radius R gobbles

up its neighboring droplets of mean radius $\langle r \rangle \ll R$ and number density (per unit area) n, the interfacial energy of the smaller droplets E_γ is released at a rate of

$$\begin{aligned}
\frac{dE_\gamma}{dt} &= (2RU_{\mathrm{L}})(2n\pi\langle r^2\rangle)\gamma \\
&= 4n\pi\langle r^2\rangle RU_{\mathrm{L}}\gamma \\
&= 4\phi_l RU_{\mathrm{L}}\gamma,
\end{aligned} \quad (1)$$

where γ is the droplet's surface tension, $\phi_l = n\pi\langle r\rangle^2$ is the *local* surface coverage of the smaller droplets approximated here as hemispheres with surface areas $2\pi\langle r^2\rangle$ and projected areas $\pi\langle r^2\rangle$. In our experiments, the lubricant oil (silicone or fluorinated) tends to wrap around the water droplet. Hence, γ is the effective surface tension whose magnitude varies between 60 and 70 mN m^{-1} depending on the choice of lubricant (see Table III in [46]).

A fraction $\alpha < 1$ of this interfacial energy is converted to translational kinetic energy, which is in turn balanced by viscous dissipation. Previously, we and others showed that the viscous force for a droplet moving on lubricated surface is given by $F_\eta = 16\gamma R\,\mathrm{Ca}^{2/3}$, where $\mathrm{Ca} = \eta U_{\mathrm{L}}/\gamma$ is the capillary number [21,22] and η the lubricant viscosity. Hence, we expect $F_\eta U_{\mathrm{L}} = 4\alpha\phi_l RU_{\mathrm{L}}\gamma$ and therefore

$$U_{\mathrm{L}} = \frac{\gamma}{\eta}\left(\frac{\alpha\phi_l}{4}\right)^{3/2}, \quad (2)$$

with γ/η being the characteristic viscocapillary speed, which is temperature-dependent (see SM Figs. S3–S5 for a rigorous justification [39]). Self-avoiding motion arises because its previous path contains little to no water content to fuel self-propulsion (i.e., $\phi_l = 0$ and hence appears white), and droplets continually seek areas with *locally* higher ϕ_l (darker regions) (SM Fig. S4, SM Video S4, and SM "Materials and Methods" section [39]).

The role of micropillars is to retain the lubricant, and U_L is insensitive to the exact texture geometries. Our model also predicts that U_L is independent of droplet radius R, which is consistent with the experimental results in Figs. 2(c) and 2(d): the droplet moves at relatively constant speed despite tripling its size. This is in sharp contrast to the *vertical* velocity of jumping droplets on superhydrophobic surfaces $U_{\mathrm{V}} \sim \sqrt{\gamma/\rho R}$, which is highly dependent on R [7]. The prediction that U_{L} increases with ϕ_l is also borne out *qualitatively* in experiments (SM Fig. S4 [39]). However, with IR imaging in Fig. 2(b) (and SM Fig. S4 [39]), ϕ_l value can only be deduced *qualitatively*.

To accurately quantify ϕ_l, we imaged the droplets using a microscope objective and a high resolution camera [Figs. 3(a), 3(b), and SM Video S5 [39]]. We observed a large droplet ($R = 1.2$ mm, circled blue) moving in a serpentine fashion, sweeping through much smaller droplets with $\langle r\rangle = 18\,\mu$m and local $\phi_l = 0.2$ [boxed green in
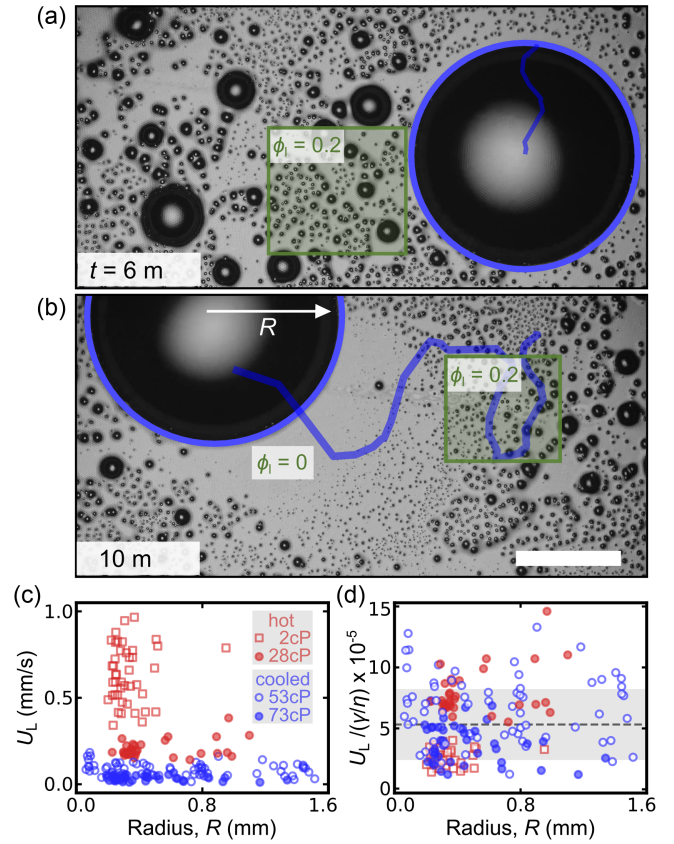

FIG. 3. (a),(b) Enlarged view of droplet with radius R sweeping through neighboring droplets of much smaller mean radius $\langle r\rangle$ and *local* area coverage ϕ_l. Scale bar is 1 mm. $t = 0$ m corresponds to start of the droplet serpentine motion. (c) Velocity U_{L} and (d) normalized velocity $U_{\mathrm{L}}/(\gamma/\eta)$ as a function of droplet radius R on lubricated surfaces with different viscosities. Circles and squares represent fluorinated and silicone oils, respectively. We used nanotextured and micropillar surfaces for hot and cooled experiments, respectively.

Fig. 3(a)]. Immediately after an area is swept through, $\phi_l = 0$ but returns to its original value within minutes of recondensation [Fig. 3(b)]. Experimentally, ϕ_l remains relatively constant at 0.15–0.30 over 4 h of continuous cooling; this saturation value is significantly lower than 0.55 typically encountered on solid surfaces [4] and results from a complex interplay between the sweeping droplet motions and the recondensation rates (SM Figs. S6,S7 [39]).

We measured U_{L} for droplets of various $R = 0.075$–1.5 mm on two surfaces with different fluorinated oils cooled to $T = 4\,°\mathrm{C}$ [blue open and filled markers in Fig. 3(c)]. We found that U_{L} remained constant at 0.09 ± 0.03, 0.04 ± 0.01 mm s^{-1} for the two cases ($\eta=53$, 73 mPa.s or cP, respectively) over 4 h of continuous cooling; more importantly, U_{L} is independent of R as predicted by Eq. (2). When hot vapor from a heated beaker of water condenses on a lubricated nanotextured surface (water and substrate temperatures $T_w = 55\,°\mathrm{C}$ and $T = 40\,°\mathrm{C}$, respectively), the condensate droplets also

Self-similar serpentine motions **Circular motions**
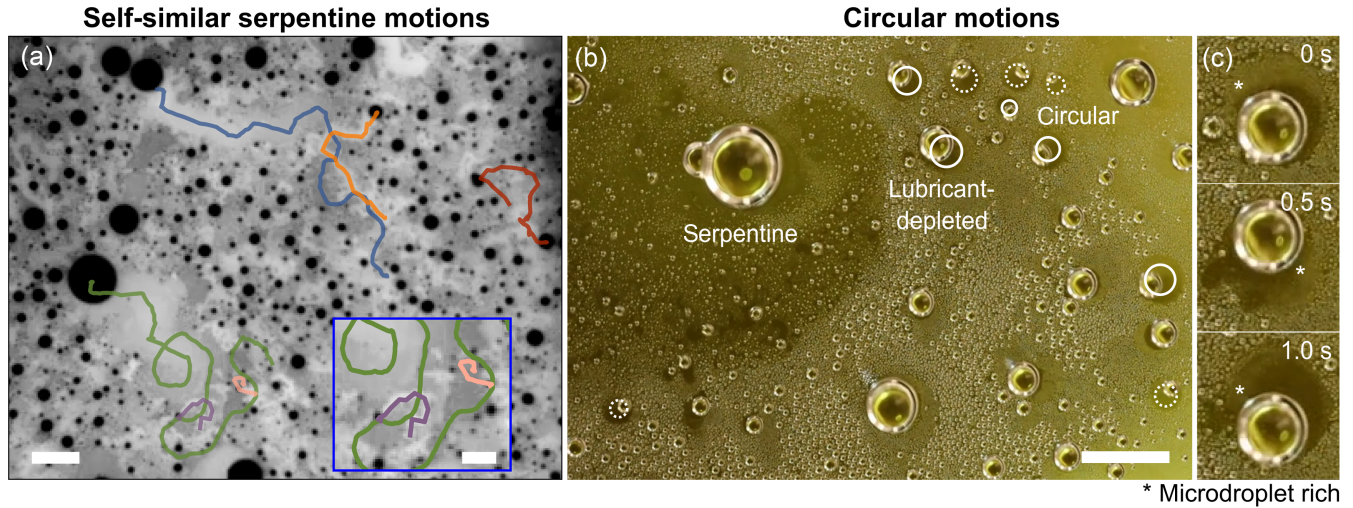

* Microdroplet rich

FIG. 4. Self-similar serpentine and circular motions of condensate droplets. (a) IR imaging of self-similar serpentine droplet motions on cooled substrate. Scale bars are 2 mm and 1 mm for main figure and inset. (b) Multiple circular motions coexist with serpentine motions for hot vapor condensates on nanotextured surface lubricated with silicone oil ($\eta = 2$ mPa.s). Clockwise and anticlockwise motions (indicated by full and dashed circles, respectively) appear with equal probability. Scale bar is 2 mm. (c) Clockwise circular motion for one droplet ($R = 0.5$ mm) in (b).

perform serpentine motion (SM Figs. S8,S9 and Video S6 [39]). The resulting propulsion speeds $U_L = 0.20 \pm 0.05$ and 0.63 ± 0.17 mm s^{-1} are similarly independent of R [red markers in Fig. 3(c)], but their magnitudes are higher because of the lower lubricant viscosities ($\eta = 28$ and 2 mPa.s^{-1}, respectively).

When scaled by the viscocapillary speed γ/η, all the velocity data overlap with one another with a mean value of $U_L/(\gamma/\eta) = (5 \pm 3) \times 10^{-5}$ [Fig. 3(d)]; the scatter in the data can be attributed to variations in local lubricant film thickness and wetting ridge geometries, which can influence viscous dissipation and are not accounted for by our model. If we compare the $U_L/(\gamma/\eta)$ value with predictions of Eq. (2) and use the fact that $\phi_l = 0.2$, we conclude that $\alpha \approx 0.03$, i.e., about 3% of the interfacial energy is converted to translational motion, with the rest likely to be converted into flow inside the droplet. Similarly low $\alpha \sim 1\%$ was reported for jumping droplets on superhydrophobic surfaces [47,48].

As the system polydispersity increased, we observed multiple droplets of different sizes ($R = 0.05$–1 mm) performing serpentine motions [Fig. 4(a) and SM Video S7 [39]]. The resulting breath figure exhibits self-similarity (at least over 1 order of magnitude), and the droplet motions look roughly similar irrespective of scale [compare inset and main image in Fig. 4(a)]. This self-similarity is a direct result of the lack of a natural length scale in the problem [49]: U_L is independent of R and depends only indirectly on $\langle r \rangle$. In contrast, there is no self-similarity in jumping droplets where $U_V \propto 1/R^{1/2}$: only small submillimetric but not large millimetric droplets jump off superhydrophic surfaces.

As time progresses, the sweeping droplet motions *locally* deplete the lubricant film [46] such that wetting ridges can no longer overlap to drive capillary attraction; in such lubricant-depleted regions, the droplets are immobile and are more uniform in size [compare left and right portions in Fig. 4(b)]. However, there are small pockets in the lubricant-depleted region with thicker lubricant overlayer where droplets ($R = 0.1$–0.5 mm) remain mobile and move in circular motions, with both clockwise and anticlockwise directions occurring with equal probability (SM Video S8 [39]). Figure 4(c) is a close-up of one such (clockwise) circular motion. The droplet ($R = 0.5$ mm) continually seeks areas with higher ϕ_l but excluding lubricant-depleted regions; the higher ϕ_l regions (indicated by asterisk) appear fuzzy because of the newly formed condensates (compare this to the clear trail left behind by the moving droplet where $\phi_l = 0$). The circular motion, which can be maintained over many cycles, is therefore similarly fueled by the same release of interfacial energy and can be thought of as a special case of serpentine motion *constrained* to areas with sufficient lubricant overlayer (SM Figs. S10, S11 [39]).

These circular motions can coexist with the self-similar serpentine motions on different areas of the same surface. As the lubricant is continually being redistributed across the substrate by the moving droplets, the various droplets continually switch between serpentine and circular motions in a highly collective fashion (SM Videos S6–S8 [39]). The collective motion will eventually stop when h_o becomes too thin for the wetting ridges of neighboring droplets to overlap (SM Fig. S11) [39]. For Figs. 3(a) and 3(b), droplet self-propulsion eventually stops after 250 m of continuous cooling (SM Fig. S12 and Video S9 [39]).

To conclude, we have described how interfacial energy release can fuel the collective motion of condensate droplets on lubricated surfaces—an interesting example of emergent behavior in active matter driven by condensation. The phenomenon described in this Letter is general and applies to different substrates (micropillars vs nanotextures) and experimental conditions (cooled substrate vs hot vapor). Different modes of droplet motion from self-similar serpentine to circular motions were observed, and we propose a simple physical model to account for the observed droplet speeds based on energy balance. Our work has potentially important heat-transfer and water-harvesting applications.

---

[*]Corresponding author: jaiz@seas.harvard.edu
[†]Corresponding author: xi.yao@cityu.edu.hk
[‡]Corresponding author: danield@kaust.edu.sa

[1] R. Lord, Breath figures, Nature (London) **86**, 416 (1911).
[2] C. V. Raman, The colours of breathed-on plates, Nature (London) **107**, 714 (1921).
[3] C. M. Knobler and D. Beysens, Growth of breath figures on fluid surfaces, Europhys. Lett. **6**, 707 (1988).
[4] D. Beysens, Dew nucleation and growth, C.R. Phys. **7**, 1082 (2006).
[5] D. Beysens, *The Physics of Dew, Breath Figures and Dropwise Condensation* (Springer, New York, 2022), Vol. 994.
[6] J. W. Rose, Dropwise condensation theory and experiment: A review, Proc. Inst. Mech. Eng. A **216**, 115 (2002).
[7] J. B. Boreyko and C.-H. Chen, Self-propelled dropwise condensate on superhydrophobic surfaces, Phys. Rev. Lett. **103**, 184501 (2009).
[8] A. Zhang, H. Bai, and L. Li, Breath figure: A nature-inspired preparation method for ordered porous films, Chem. Rev. **115**, 9801 (2015).
[9] A. E. Goodling, S. Nagelberg, B. Kaehr, C. H. Meredith, S. I. Cheon, A. P. Saunders, M. Kolle, and L. D. Zarzar, Colouration by total internal reflection and interference at microscale concave interfaces, Nature (London) **566**, 523 (2019).
[10] S. Anand, A. T. Paxson, R. Dhiman, J. D. Smith, and K. K. Varanasi, Enhanced condensation on lubricant-impregnated nanotextured surfaces, ACS Nano **6**, 10122 (2012).
[11] S. Anand, K. Rykaczewski, S. B. Subramanyam, D. Beysens, and K. K. Varanasi, How droplets nucleate and grow on liquids and liquid impregnated surfaces, Soft Matter **11**, 69 (2015).
[12] R. Xiao, N. Miljkovic, R. Enright, and E. N. Wang, Immersion condensation on oil-infused heterogeneous surfaces for enhanced heat transfer, Sci. Rep. **3**, 1988 (2013).
[13] J. Sun and P. B. Weisensee, Microdroplet self-propulsion during dropwise condensation on lubricant-infused surfaces, Soft Matter **15**, 4808 (2019).
[14] J. Sun and P. B. Weisensee, Marangoni-induced reversal of meniscus-climbing microdroplets, Soft Matter **19**, 625 (2023).
[15] K.-C. Park, P. Kim, A. Grinthal, N. He, D. Fox, J. C. Weaver, and J. Aizenberg, Condensation on slippery asymmetric bumps, Nature (London) **531**, 78 (2016).
[16] S. Adera, L. Naworski, A. Davitt, N. K. Mandsberg, A. V. Shneidman, J. Alvarenga, and J. Aizenberg, Enhanced condensation heat transfer using porous silica inverse opal coatings on copper tubes, Sci. Rep. **11**, 10675 (2021).
[17] A. Tripathy, C. W. E. Lam, D. Davila, M. Donati, A. Milionis, C. S. Sharma, and D. Poulikakos, Ultrathin lubricant-infused vertical graphene nanoscaffolds for high-performance dropwise condensation, ACS Nano **15**, 14305 (2021).
[18] A. Lafuma and D. Quéré, Slippery pre-suffused surfaces, Europhys. Lett. **96**, 56001 (2011).
[19] T.-S. Wong, S. H. Kang, S. K. Y. Tang, E. J. Smythe, B. D. Hatton, A. Grinthal, and J. Aizenberg, Bioinspired self-repairing slippery surfaces with pressure-stable omniphobicity, Nature (London) **477**, 443 (2011).
[20] J. D. Smith, R. Dhiman, S. Anand, E. Reza-Garduno, R. E. Cohen, G. H. McKinley, and K. K. Varanasi, Droplet mobility on lubricant-impregnated surfaces, Soft Matter **9**, 1772 (2013).
[21] D. Daniel, J. V. I. Timonen, R. Li, S. J. Velling, and J. Aizenberg, Oleoplaning droplets on lubricated surfaces, Nat. Phys. **13**, 1020 (2017).
[22] A. Keiser, P. Baumli, D. Vollmer, and D. Quéré, Universality of friction laws on liquid-infused materials, Phys. Rev. Fluids **5**, 014005 (2020).
[23] D. Vella and L. Mahadevan, The "cheerios effect", Am. J. Phys. **73**, 817 (2005).
[24] J. Jiang, J. Gao, H. Zhang, W. He, J. Zhang, D. Daniel, and X. Yao, Directional pumping of water and oil microdroplets on slippery surface, Proc. Natl. Acad. Sci. U.S.A. **116**, 2482 (2019).
[25] H. Xu, Y. Zhou, D. Daniel, J. Herzog, X. Wang, V. Sick, and S. Adera, Droplet attraction and coalescence mechanism on textured oil-impregnated surfaces, Nat. Commun. **14**, 4901 (2023).
[26] J. Aizenberg, P. V. Braun, and P. Wiltzius, Patterned colloidal deposition controlled by electrostatic and capillary forces, Phys. Rev. Lett. **84**, 2997 (2000).
[27] T. O'Connor, Emergent properties, in *The Stanford Encyclopedia of Philosophy*, Winter 2021 ed., edited by Edward N. Zalta (Metaphysics Research Lab, Stanford University, Stanford, California, 2021).
[28] P. W. Anderson, More is different: Broken symmetry and the nature of the hierarchical structure of science. Science **177**, 393 (1972).
[29] T. Sanchez, D. T. N. Chen, S. J. DeCamp, M. Heymann, and Z. Dogic, Spontaneous motion in hierarchically assembled active matter, Nature (London) **491**, 431 (2012).
[30] T. Vicsek and A. Zafeiris, Collective motion, Phys. Rep. **517**, 71 (2012).

[31] S. Michelin, Self-propulsion of chemically active droplets, Annu. Rev. Fluid Mech. **55**, 77 (2023).

[32] A. Steyer, P. Guenoun, and D. Beysens, Spontaneous jumps of a droplet, Phys. Rev. Lett. **68**, 64 (1992).

[33] Z. Izri, M. N. Van Der Linden, S. Michelin, and O. Dauchot, Self-propulsion of pure water droplets by spontaneous Marangoni-stress-driven motion, Phys. Rev. Lett. **113**, 248302 (2014).

[34] C. H. Meredith, P. G. Moerman, J. Groenewold, Y.-J. Chiu, W. K Kegel, A. van Blaaderen, and L. D. Zarzar, Predator–prey interactions between droplets driven by non-reciprocal oil exchange, Nat. Chem. **12**, 1136 (2020).

[35] Y. Wen, P. Y. Kim, S. Shi, D. Wang, X. Man, M. Doi, and T. P. Russell, Vapor-induced motion of two pure liquid droplets, Soft Matter **15**, 2135 (2019).

[36] X. Liu, N. Kent, A. Ceballos, R. Streubel, Y. Jiang, Y. Chai, P. Y. Kim, J. Forth, F. Hellman, S. Shi, D. Wang, B. A. Helms, P. D. Ashby, P. Fischer, and T. P. Russell, Reconfigurable ferromagnetic liquid droplets, Science **365**, 264 (2019).

[37] W. F. Paxton, S. Sundararajan, T. E. Mallouk, and A. Sen, Chemical locomotion, Angew. Chem., Int. Ed. **45**, 5420 (2006).

[38] L. Limozin and K. Sengupta, Quantitative reflection interference contrast microscopy (RICM) in soft matter and cell adhesion, ChemPhysChem **10**, 2752 (2009).

[39] See Supplemental Material at http://link.aps.org/supplemental/10.1103/PhysRevLett.132.058203 for details of materials and methods and further analysis, which includes Ref. [40].

[40] D. S. Bodas, A. B. Mandale, and S. A. Gangal, Deposition of PTFE thin films by RF plasma sputtering on ⟨100⟩ silicon substrates, Appl. Surf. Sci. **245**, 202 (2005).

[41] J. B. Boreyko, G. Polizos, P. G. Datskos, S. A. Sarles, and C. P. Collier, Air-stable droplet interface bilayers on oil-infused surfaces, Proc. Natl. Acad. Sci. U.S.A. **111**, 7588 (2014).

[42] G. Bradski, The OpenCV Library, Dr. Dobb's Journal of Software Tools (2000).

[43] P. B. Weisensee, H. Wang, Y.and Qian, D. Schultz, W. P. King, and N. Miljkovic, Condensate droplet size distribution on lubricant-infused surfaces, Int. J. Heat Mass Transfer **109**, 187 (2017).

[44] P. A. Kralchevsky and K. Nagayama, Capillary interactions between particles bound to interfaces, liquid films and biomembranes, Adv. Colloid Interface Sci. **85**, 145 (2000).

[45] D. Y. C. Chan, J. D. Henry Jr, and L. R. White, The interaction of colloidal particles collected at fluid interfaces, J. Colloid Interface Sci. **79**, 410 (1981).

[46] M. J. Kreder, D. Daniel, A. Tetreault, Z. Cao, B. Lemaire, J. V. I. Timonen, and J. Aizenberg, Film dynamics and lubricant depletion by droplets moving on lubricated surfaces, Phys. Rev. X **8**, 031053 (2018).

[47] R. Enright, N. Miljkovic, J. Sprittles, K. Nolan, R. Mitchell, and E. N. Wang, How coalescing droplets jump, ACS Nano **8**, 10352 (2014).

[48] X. Yan, L. Zhang, S. Sett, L. Feng, C. Zhao, Z. Huang, H. Vahabi, A. K. Kota, F. Chen, and N. Miljkovic, Droplet jumping: Effects of droplet size, surface structure, pinning, and liquid properties, ACS Nano **13**, 1309 (2019).

[49] B. B Mandelbrot, *The Fractal Geometry of Nature* (W.H. Freeman, New York, 1982), Vol. 1.